ARMA 14-7040

SAND2014-1623C

Potential Use of Geologic Rock Salt for Fuel Cycle Sustainability – a Computational Modeling Perspective

Argüello, J.G.
Sandia National Laboratories, Albuquerque, NM, USA

This paper was prepared for presentation at the 48th US Rock Mechanics / Geomechanics Symposium held in Minneapolis, MN, USA, 1-4 June 2014.

ABSTRACT: Because of relatively recent decisions by the current administration and its renewed assessment of the nuclear life-cycle, the various deep geologic disposal medium options are once again open for consideration. This paper focuses on addressing the favorable creep properties and behavior of rock salt, from the computational modeling perspective, as it relates to its potential use as a disposal medium for a deep geologic repository. The various components that make up a computational modeling capability to address the thermo-mechanical behavior of rock salt over a wide range of time and space are presented here. Several example rock salt calculations are also presented to demonstrate the applicability and validity of the modeling capability described herein to address repository-scale problems. The evidence shown points to a mature computational capability that can generate results relevant to the design and assessment of a potential rock salt HLW repository.

1. INTRODUCTION

Commercial U.S. nuclear power plants produce more than 20% of the electrical power for the nation and in the process generate more than 2000-2300 metric tons of used fuel per year [1]. For multiple decades, nuclear waste has been accumulating from the nation's commercial nuclear power plants. The need for the permanent geologic disposal of these wastes to allow for the long-term sustainability of the nuclear fuel cycle has long been recognized as being part of an integrated fuel management strategy. In fact, formal studies in the U.S. that addressed the question of which disposal medium in geologic structures would be best for the permanent storage (disposal) of nuclear wastes began in the mid-1950s. At the time, the U.S. Atomic Energy Commission (now the U.S. Department of Energy [DOE]) asked the National Academy of Sciences to establish a committee of earth scientists to study the problem [2]. That committee concluded that natural underground rock salt formations are among the most favorable disposal environments. The favorability of rock salt comes from the following reasons:

- Rock salt is almost impermeable – a deposit's very existence implies the absence of circulating groundwater and of dissolution;
- It slowly deforms under stress (creeps) to prevent or heal openings that could otherwise release radioactivity into the environment;
- It readily dissipates the heat from nuclear wastes;
- It occurs widely throughout the U.S.; and
- Rock salt is easy to mine; yet it's strong enough to allow the creation of large rooms for accommodating disposal.

Because of relatively recent decisions by the current administration and its renewed assessment of the nuclear life-cycle, the various deep geologic disposal medium options are once again open for consideration [3]. This paper focuses on addressing the favorable properties and behavior of rock salt, from the computational modeling perspective, as it relates to its potential use as a disposal medium for a deep geologic repository.

2. MODELS AND TOOLS FOR USE IN THE DEVELOPMENT OF A REPOSITORY

Development of a repository to assure adequate containment and isolation of the radioactive wastes requires a design basis and experience that have both been validated through demonstrations in-situ. There are several key factors in the development of a repository, including (1) a sound design of the system; (2) validated computational models and tools to permit crafting system designs with confidence; and (3) acceptable techniques for evaluating (assessing) the design's performance by methods known to be valid [4]. The focus of this work will be from the perspective of the validated tools and models for use in the design and assessment of a potential rock salt repository. We will address the thermo-mechanical (TM) aspects of the problem, specifically, and also touch upon some open questions that still remain to be answered, which may potentially include thermo-hydro-mechanical (THM) couplings to adequately address them.

The various components that make up a computational modeling capability to address the thermo-mechanical behavior of rock salt over a wide range of time and space will first be presented. The solver technology that is required to address the large deformation, highly nonlinear, nature of the repository will be addressed, in general. Included will be the features of a valid constitutive model needed to capture the important phenomena of rock salt creep deformation over repository performance ranges. Also in this discussion will be the typical issues of importance in computational models, i.e., discretization, stability, accuracy, etc.

Confidence in computational models is attained by grounding the models on sound physical principles, first, and then using acceptable mathematical and numerical methods to represent the behavior. They are then validated through a systematic process that includes exercising the model to solve a basic problem (one with a known solution, if possible); comparing model response against behavior of natural known phenomena; conducting laboratory, bench-scale, and field tests to evaluate the performance of the model's predictions; and conducting in-situ tests to compare predictive results of the model with actual underground data. Hence, several example rock salt calculations will be presented to demonstrate the applicability and validity of the modeling capability described here to repository-scale problems. These will vary from simple problems designed to test elementary creep response behavior to the more complex that deal with addressing specific aspects of repository room behavior. Finally a summary and a set of conclusions will be offered for the reader's consideration relative to the state of computational modeling of rock salt and its applicability to the problem of radioactive waste disposal in rock salt for fuel cycle sustainability.

3. COMPUTATIONAL CAPABILITY FOR MODELING GEOLOGIC ROCK SALT

In this section, the components that make up a geomechanical computational modeling capability for geologic rock salt are presented; namely, the governing thermo-mechanical equations, the constitutive model, and discretization/solution technique used to solve the equations. Much of what follows in this section is gleaned from Sandia National Laboratories' extensive historical experience in its various roles with the Waste Isolation Pilot Plant (WIPP) project and the author's approximately 30-year involvement, in a computational mechanics support role, on this and other projects at Sandi in which predicting rock salt thermo-mechanical behavior was important.

3.1. Governing Mechanical Equations

For mechanical (geo-mechanical) systems, there are three basic sets of equations that govern the response of the system deforming under a given load. The first set is the set of equations of motion:

$$\sigma_{ij,j} + \rho b_j = \rho a_j \tag{1}$$

or, for the case when the processes are very slow such that inertia (ρa_j), may be neglected, these equations become the equilibrium equations:

$$\sigma_{ij,j} + f_i = 0 \tag{2}$$

where σ_{ij} are the components of the stress tensor and $f_i = \rho b_i$ are the body forces, with ρ being the density. The second set is the set of strain-displacement relations:

$$e_{ij} = \frac{1}{2}\left(u_{i,j} + u_{j,i} + u_{k,j}u_{k,i}\right) \tag{3}$$

where e_{ij} is the strain tensor and u_i is the displacement vector.

The third set of equations, the so-called constitutive equations, relates the equilibrium equations to the strain-displacement relations through the material (constituent) response of that material undergoing the deformations. This third set of equations can take on many forms depending on the material that is being modeled, ranging all the way from a simple elastic material that could be used to model, say a granitic material, to materials such as clay and rock salt, with significantly more complex behaviors that require more sophisticated and involved material descriptions. For the present work, we consider a constitutive model for rock salt. This is one of the materials of interest for nuclear fuel cycle sustainability and is a creeping material with a creep rate that is highly temperature-dependent. Its overall strain rate can be characterized by the equation:

$$\dot{e}_{ij} = -\frac{\nu}{E}\dot{\sigma}_{kk}\delta_{ij} + \frac{1+\nu}{E}\dot{\sigma}_{ij} + \dot{e}^{c}_{ij} + 3\alpha\dot{T}\delta_{ij} \tag{4}$$

where ν is the Poisson's ratio, E is Young's Modulus, T is temperature ($^\circ K$), α is the coefficient of linear thermal expansion, and δ_{ij} is the Kronecker Delta. Of course, the temperature in this equation is solved for, as well, incorporating the appropriate heat transfer processes occurring in the configuration of interest underground but the details of this will not be addressed here and it will be assumed that the temperature history is known. The creep model is thus embodied within the third term on the right-hand-side of Eq. (4) and the following subsection describes the MD creep model, a model that has been extensively used in the U.S. to model rock salt behavior [5].

3.2. *Multi-mechanism Deformation Creep Model*

The Multimechanism Deformation (MD) creep model was originally developed by Munson and Dawson [6,7, 8] and later extended by Munson et al. [9]. The MD model mathematically represents the primary and secondary creep behavior of salt due to dislocations under relatively low temperatures (compared to the melting temperature) and low to moderate stresses which are typical of mining and storage cavern operations. Three micromechanical mechanisms, determined from deformation mechanism maps [10], are represented in the model: 1) a dislocation climb mechanism active at high temperatures and low stresses, 2) an empirically observed but undefined mechanism active at low temperatures and low stresses, and 3) a dislocation slip mechanism active at high stresses. These creep mechanisms are assumed to act such that the total steady state creep rate can be written as the sum of the individual mechanism strain rates.

$$\dot{\varepsilon}_s = \sum_{i=1}^{3} \dot{\varepsilon}_{s_i} \tag{5}$$

The influence of temperature on the creep strain rate is included through an Arrhenius term. The steady state creep strain rates for the first and second mechanisms are identical in form and are implemented using a power law model while the third mechanism (dislocation slip) is represented using an Eyring type model.

$$\dot{\varepsilon}_{s_1} = A_1 \left(\frac{\sigma_{eq}}{G} \right)^{n_1} e^{\frac{-Q_1}{RT}} \tag{6}$$

$$\dot{\varepsilon}_{s_2} = A_2 \left(\frac{\sigma_{eq}}{G} \right)^{n_2} e^{\frac{-Q_2}{RT}} \tag{7}$$

$$\dot{\varepsilon}_{s_3} = \left(B_1 e^{-Q_1/RT} + B_2 e^{-Q_2/RT} \right) \sinh\left[q \left(\frac{\sigma_{eq} - \sigma_0}{G} \right) \right] H\left(\sigma_{eq} - \sigma_0\right) \tag{8}$$

where:

σ_{eq} = equivalent stress

A_i and B_i = structure factors

Q_i = activation energies

T = absolute temperature

G = shear modulus

R = universal gas constant

n_i = stress exponents

q = stress constant

σ_0 = stress limit of the dislocation slip mechanism

|H| = Heaviside function with the argument $(\bar{\sigma} - \sigma_0)$

From the definition of the Heaviside function, the third mechanism is only active when the equivalent stress exceeds the specified value of the stress limit σ_0. The equivalent stress appearing in these equations is taken to be the Tresca stress [9]. The Tresca stress can be written in terms of the maximum and minimum principal stresses σ_1 and σ_3, respectively with $(\sigma_1 \geq \sigma_2 \geq \sigma_3)$. Alternatively, the Tresca stress may be written as a function of the Lode angle ψ and the second invariant J_2 of the deviatoric stress tensor **s** (whose components are s_{ij}).

$$\sigma_{eq} = \sigma_1 - \sigma_3 = 2\cos\psi\sqrt{J_2} \tag{9}$$

The Lode angle is dependent on both the second and third invariant, J_3, of the deviatoric stress tensor s_{ij}.

$$\psi = \frac{1}{3}\sin^{-1}\left[\frac{-3\sqrt{3}J_3}{2J_2^{3/2}} \right] \quad -\frac{\pi}{6} \leq \psi \leq \frac{\pi}{6} \tag{10}$$

$$J_2 = \frac{1}{2} s_{ij} s_{ij} \tag{11}$$

$$J_3 = \frac{1}{3} s_{ij} s_{jk} s_{ki} \tag{12}$$

The kinetic equation used in the MD model is given by Eq. (13) where F is a function which accounts for transient creep effects and $\dot{\varepsilon}_s$ is the steady state dislocation creep strain rate defined by Eq. (5).

$$\dot{\varepsilon}_{eq} = F\dot{\varepsilon}_s \tag{13}$$

The function F has three branches: a work hardening branch ($F > 1$), an equilibrium branch ($F = 1$), and a recovery branch ($F < 1$).

$$
F = \begin{cases} \exp\left[\Delta\left(1-\dfrac{\zeta}{\varepsilon_t^f}\right)^2\right] & \zeta < \varepsilon_t^f \quad \text{Transient Branch} \\ 1 & \zeta = \varepsilon_t^f \quad \text{Equilibrium Branch} \\ \exp\left[-\delta\left(1-\dfrac{\zeta}{\varepsilon_t^f}\right)^2\right] & \zeta > \varepsilon_t^f \quad \text{Recovery Branch} \end{cases} \tag{14}
$$

The choice of the particular branch depends on the transient strain limit ε_t^f and the internal variable ζ. The transient strain limit is defined by Eq. (15) where K_0, c, and m are material parameters, T is the absolute temperature, and G is the shear modulus.

$$
\varepsilon_t^f = K_0 e^{cT}\left(\frac{\sigma_{eq}}{G}\right)^m \tag{15}
$$

The internal variable ζ, appearing in the calculation of the function F, is obtained by integration of the evolution equation

$$
\dot{\zeta} = \left(F-1\right)\dot{\varepsilon}_s \tag{16}
$$

Δ and δ, appearing in Eq. (14), are the work hardening and recovery parameters and are given by Eqs. (17) and (18) respectively. In these equations α, β, α_r, and β_r are material parameters. Typically the recovery parameter δ is taken to be constant (i.e. $\delta = \alpha_r$).

$$
\Delta = \alpha + \beta \log\left(\frac{\sigma_{eq}}{G}\right) \tag{17}
$$

$$
\delta = \alpha_r + \beta_r \log\left(\frac{\sigma_{eq}}{G}\right) \tag{18}
$$

For three dimensional states of stress the components of the creep strain rate tensor are generalized [11] as

$$
\dot{\varepsilon}_{ij}^c = \dot{\varepsilon}_{eq}\frac{\partial \sigma_{eq}}{\partial \sigma_{ij}} \tag{19}
$$

Using the Tresca stress, Eq. (9), as the equivalent stress in this form means the creep strains are purely deviatoric ($\dot{\varepsilon}_{ij}^c = \dot{e}_{ij}^c$ since $\dot{\varepsilon}_{kk}^c = 0$) and that all volume change is elastic as defined though the bulk modulus K (i.e. $\varepsilon_{kk} = {}^{\sigma_{kk}}\!/_{3K}$). Therefore Eq. (19) becomes

$$
\dot{e}_{ij}^c = \dot{\varepsilon}_{eq}\frac{\partial \sigma_{eq}}{\partial \sigma_{ij}} = \dot{\varepsilon}_{eq} N_{ij} \tag{20}
$$

Including the bulk and shear moduli, which are both assumed constant, there are a total of 20 parameters used to define the MD model. Typical material parameters for WIPP clean salt (Halite) for use with the MD model are given in Table 2. Some of the parameters have different values for Argillaceous Salt (Halite) also found at WIPP and are shown in parenthesis in the table.

If only the steady state creep response is of interest then the transient and recovery branches may be effectively turned off by setting $\alpha = 0$, $\beta = 0$, $\alpha_\gamma = 0$, $\beta_\gamma = 0$.

The MD model can be further simplified to that of a power law creep model by setting the appropriate structure factors and activation energies to zero. The scalar secondary creep strain rate for a power law creep model is given by:

Table 1. Typical material properties for WIPP salt used with the MD model

	Parameters		Units	Salt
Elastic Properties	Shear modulus	G	MPa	12,400
	Young's modulus	E	MPa	31,000
	Poisson's ratio	ν	–	0.25
Salt Creep Properties	Structure Factors	A_1	s^{-1}	8.386×10^{22} (1.407×10^{23})
		B_1		6.086×10^{6} (8.998×10^{6})
		A_2		9.672×10^{12} (1.314×10^{13})
		B_2		3.034×10^{-2} (4.289×10^{-2})
	Activation energies	Q_1	cal/mole	25,000
		Q_2	cal/mole	10,000
	Universal gas constant	R	cal/mol-°K	1.987
	Absolute temperature	T	°K	300
	Stress exponents	n_1	–	5.5
		n_2		5.0
	Stress limit of the dis-location slip mechanism	σ_0	MPa	20.57
	Stress constant	q	–	5,335
	Transient strain limit constants	M	–	3.0
		K_0	–	6.275×10^{5} (2.470×10^{6})
		c	$°K^{-1}$	9.198×10^{-3}
	Constants for work-hardening parameter	α	–	-17.37 (-14.96)
		β	–	-7.738
	Recovery parameter	δ	–	0.58

$$\dot{\varepsilon}_s = Ae^{-Q/RT}\left(\frac{\sigma_{eq}}{G}\right)^n \tag{21}$$

where σ_{eq} is the Von Mises equivalent stress.

3.3. Discretization and Solution of Equations

The governing equations described in the previous subsections are, of course, then discretized and solved numerically. Typically this is done within a displacement based finite element method (FEM) computer code. Over the decades, at Sandia, several generations of successively more-sophisticated large-displacement non-linear finite element codes have been developed to solve the highly nonlinear systems of equations typical used for rock salt as described herein. The current generation of codes is known as Sierra Mechanics [12].

The discretized version of the field equations governing deformation of the salt body can be written as:

$$\left\{\sum_N \int_{ve} B\sigma dV\right\} = \{F\} \tag{22}$$

Where the term on the left-hand side of the equation is the internal force vector and $\{F\}$ is the external force vector. B is the strain-displacement transformation matrix; N is the number of elements in the discretization; σ is an ordered vector of stress components in each element at a Gauss point, and ve is the volume of each element. As previously noted, the constitutive model (strain-displacement relationship) is incorporated via the integrand product in the left-hand side of the equation. An explicit FEM technology has historically been used at Sandia for the solution of Eq. (22) that is different from traditional FEM technology. First, a global stiffness matrix is never formed. Instead at the element level, the divergence of the stress is found, and the contributions to each node in the overall structure are summed (i.e., the vector described by the left side of the equation). A residual force vector comprised of the internal minus the external forces,

$$\{R\} = \left\{\sum_N \int_{ve} B\sigma dV\right\} - \{F\}, \tag{23}$$

is computed, and the solution procedure is then one of reducing the residual to zero using an iterative technique. Because the quantities being manipulated are vectors, there is no need to store a global stiffness matrix and factor it. Consequently the storage requirements are small when compare to the traditional FEM approach and larger problems can be solved more efficiently. The iterative techniques that have been historically used are the pre-conditioned Conjugate Gradient (CG) technique, e.g., [13] and, in the older codes, an adaptive Dynamic Relaxation (DR) technique, e.g., [14].

Historically the creep models included in the material libraries of the quasi-static finite element codes at Sandia have used forward Euler integration with an adaptive global time-stepping scheme. This adaptive scheme is key in permitting the capability to be able to model rock salt behavior out to the requisite times (thousands of years) needed for repository applications. Sub-stepping is often needed when the global time step, chosen based on accuracy conditions, is larger than the time step required for stability. Frequently it is necessary to start a simulation with a small time step in order to accurately represent the primary creep behavior (e.g., 10^{-6} s). An added benefit of using a small step size is that it often reduces the number of iterations the nonlinear conjugate gradient solver needs to satisfy equilibrium of the system.

4. BUILDING CONFIDENCE IN THE COMPUTATIONAL CAPABILITY

A series of example problems demonstrating the modeling of successively more complex rock salt behavior is presented in this section. These examples, which are of course not all-inclusive of problems that have been solved for this purpose, simply serve to demonstrate how confidence in the computational capability is systematically and eventually achieved.

4.1. Comparison to Analytic Solutions

The first example is one that tests the computational capability by analyzing a creep relaxation problem. A stress-free, isotropic, and homogeneous block of rock salt, prevented from vertical movement at the bottom, undergoes a vertical displacement δ at the top at time zero, with the sides free to deform. The simulation determines the creep stress relaxation in the block over time when δ is kept constant. Because an analytic solution is available when one assumes Norton power law secondary creep, for this problem no primary creep is included.

Recall that the total strain rate can be decomposed into elastic and creep portions. Because the displacement in the vertical direction is applied initially and then kept constant thereafter, the elastic component of the vertical strain rate is simply equal to the negative of the vertical creep rate,

$$\dot{\varepsilon}_{el} = -\dot{\varepsilon}_c \text{ or } -\frac{\dot{\sigma}}{E} = \dot{\varepsilon}_c = D\sigma^n e^{-Q/RT} \tag{24}$$

where D can be obtained by examination of Eq. (21). This equation is an ordinary differential equation for which a closed-form solution can be found by the method of separation of variables. The solution is given by:

$$\sigma(t) = \left[\sigma^{1-n}(0) + EDe^{-Q/RT}(n-1)t\right]^{1/(1-n)} \quad (25)$$

where $\sigma(t)$ is the vertical stress as a function of time and $\sigma(0)$ is the elastic vertical stress value induced initially by the application of the displacement δ. This verification problem has been used since the earliest generation of codes, even before the development of the MD creep model. Hence, specific values consistent with an earlier reference creep model [15] are used in this example and are: $\delta = 0.001$, $E = 24.75 \times 10^9$, $\nu = 0$, $D = 5.79 \times 10^{-36}$, $n = 4.9$, and $Q/(RT) = 20.13$, where units are in SI. Figure 1 shows a plot of the von Mises stress with time, $\sigma(t)$, computed with the Sierra Solid Mechanics (Adagio) code compared to the analytic solution. The figure shows the simulation tracking the analytic solution very closely and thus verifies that the implementation of, at least, the power law creep portion of the creep model is functioning as intended.

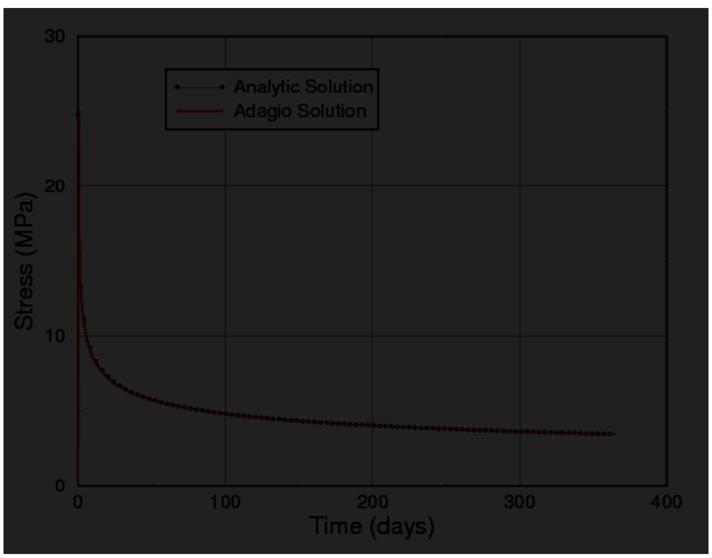

Fig. 1. Solution of Creep Stress Relaxation Problem.

While it is worthwhile to compare the capability to an analytic solution on problems where there are known solutions, there are very few such problems. So confidence has to be achieved by additional means, such as comparison with measurements. In comparing with measurements, it is useful to start at the laboratory-scale, then proceed to the bench-scale, and finally to the full-scale.

4.2. Comparisons to Lab and Bench Scale Tests

Typically laboratory tests on rock salt specimens are used for dual purposes. First for the determination of one unique salt-type specific set of model parameter values for use with the constitutive model in question and then subsequently to re-calculate the entire suite of laboratory tests with this unique set of parameters that was determined. This provides a preliminary assessment of whether the model can effectively predict the behavior seen in laboratory tests or not, over the range of stresses, temperatures, and loading rates covered by the testing. This is essential during the development of the model and has been done for the current capability (e.g., triaxial compression creep tests [16]).

At the next scale, the bench-scale is where additional complexity enters. In the laboratory, the environment that the rock salt sees during testing can be carefully controlled, but at the bench-scale, such careful control is typically no longer possible.

This next example looks at the isothermal response of a 0.315 m diameter borehole at a depth of 1042 m below the surface in the Asse Mine, Germany. The borehole was dry-drilled in December 1979 from a chamber at the 750 m level down to a depth of 1050 m below ground [17]. Three days after the deepest point of drilling was reached, on Dec. 21st, the Netherlands Energy Foundation ECN started Isothermal Free Convergence (IFC) measurements in the unconstrained and unheated borehole at a depth of 292 m (the rock salt temperature is 42 °C at this depth); the measurements were continued for 830 days until March 30, 1982 [17].

Figure 2 shows the idealized configuration and the mesh used in this Sierra Mechanics calculation. In this calculation the MD parameters used [18] are those for Asse Speisesalz. Figure 3 shows the simulation result compared to the data and indicates that with appropriate adjustment of single parameter in the MD creep model [18], the isothermal convergence of the borehole can be appropriately captured.

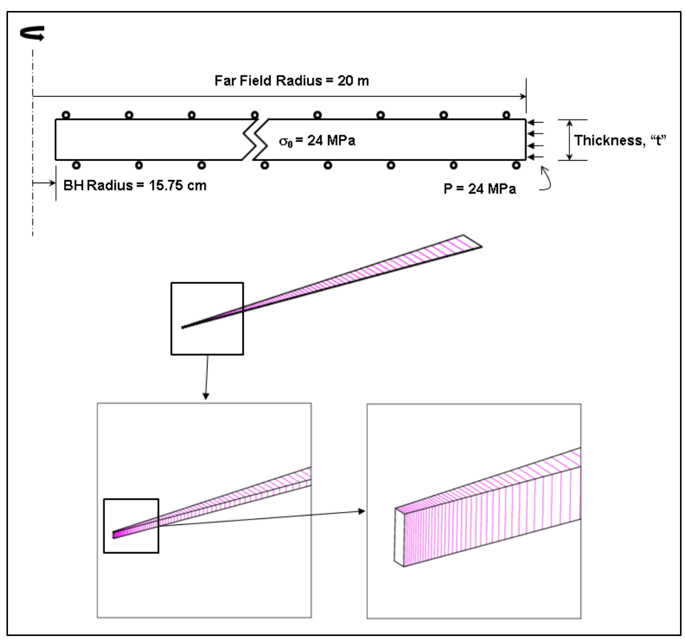

Fig. 2. IFC 5° Isothermal Wedge Slice Model Used for Borehole Simulation.

In the previous examples, the computational capability has been exercised on isothermal rock salt. However, in a repository setting, the capability needs to be able to model non-isothermal conditions as well. This next example is one that looks at the same borehole as the previous example, but for a test conducted later in time, which included heating of the borehole, the Heated Free-Convergence Probe (HFCP) experiment. This problem is part of an international benchmark project so additional details of this work can be found in [18] and comparison with results of others elsewhere [19].

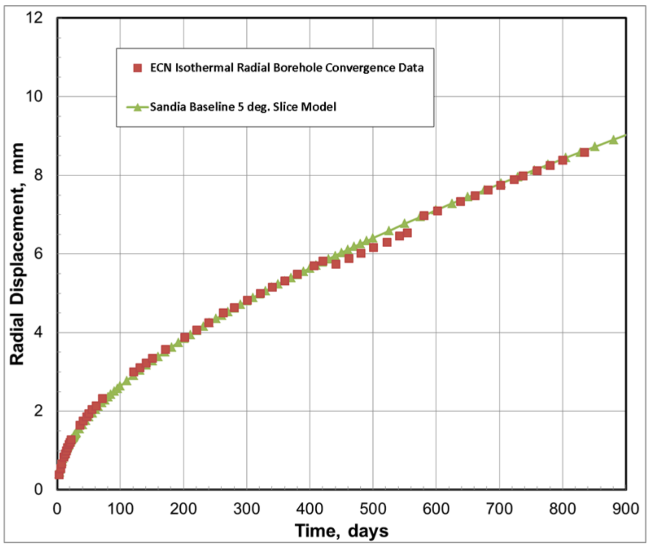

Fig. 3. IFC 5° Isothermal Wedge Slice Model Results vs. Measurements.

In July 1983, 1309 days after the end of drilling of the borehole, three heaters with a total height of 3 m were switched on in the Asse borehole. The vertical center of the three heaters was at a depth of -231 m (981 m below ground). After 19 days, with free convergence of the borehole occurring during that period, the heaters were turned off because the probe was about to come in contact with the borehole wall. ECN continued the free convergence measurements in a subsequent cool-down phase for an additional three days. Thus, the experiment ended 22 days after the start of heating.

Figure 4 shows the idealized configuration and the mesh used in this Sierra Mechanics calculation. Because the HFCP experiment was located 62 m higher in the borehole than the IFC experiment, the boundary conditions for this calculation had to be modified. A smaller hydrostatic primary stress of 23 MPa from the overburden was assumed. A smaller initial salt temperature of 313.95 K (40.8° C) with a temperature gradient of 0.02 K/m in depth was applied. A wedge-shaped calculational model with an outer radius of 20 m, a height of 20 m with the center at borehole depth 231 m, and a borehole radius of 15.75 cm was used. The simulation was performed with the same unique set of parameter values determined from the Asse Speisesalz lab test results and the further fine-tuning by means of the in-situ measured IFC data [18]. The isothermal free borehole convergence in the initial 1309 days between the drilling of this bore-hole depth and the start of heating were included in the calculations to get the correct initial conditions for the subsequent coupled thermo-mechanical simulation of the heated borehole. The reported temperature history, from the experiment, due to the three heaters was simplified. It was applied directly to the borehole wall in the 3 m high heated section as a temperature boundary condition.

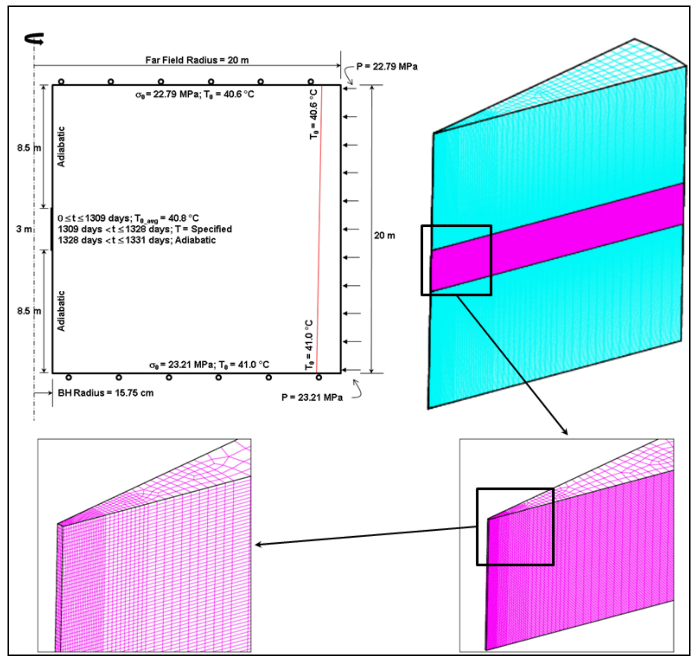

Fig. 4. HFCP 15° Non-Isothermal Wedge Model Used for Borehole Simulation.

Figure 5 shows the simulation result compared to the data at the end of heating. While the simulation slightly over-predicts the measured convergence, which may be in part due to inherent assumptions that went into the model, the figure demonstrates that the free convergence of the borehole resulting from non-isothermal loading conditions can be well-captured with the computational capability.

4.3. Comparisons to Full-Scale Tests

Although smaller-scale tests are useful for systematically building confidence in the tools, ultimate confidence in the capability of a computational model to predict repository behavior must be demonstrated by reasonable comparison to in-situ full-scale experimental data. The final example presented here deals with the simulation of a field test to evaluate the performance of the model's predictive capability. The full-scale experiment of interest here is one that was fielded in the early 1980's at the WIPP. Though isothermal, this room brings additional complexity into the simulation through the bedding clay seams and multiple materials present in the stratigraphy that need to be included in the simulation.

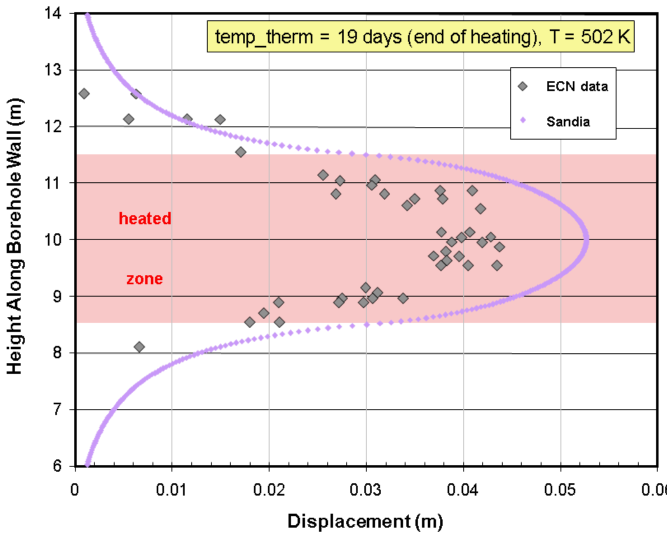

Fig. 5. HFPC 15° Non-Isothermal Wedge Model Results vs. Measurements.

The isothermal WIPP Mining Development Test (Room D) consists of a test room set into the bedded stratigraphy of the natural salt formation. The room was constructed to be thermally and structurally isolated from the other test rooms by a large pillar, approximately 79 m thick. The room has a total length of 93.3 m. The test section of the room consists of the central 74.4 m of the room and has cross section dimensions of 5.5 m wide by 5.5 m high. The Room D coordinate center is at a depth of 646.0 m below the ground surface. Details of the mining of the room and of the measurements that were taken were carefully documented [20]. The roof of Room D follows a parting defined by a small clay seam. This seam (Clay I), along with the rest of the clay seams, and the remainder of the stratigraphy around the room are shown in Figure 6.

According to Munson and co-workers [9], the clay seams noted in the stratigraphy are not in actuality distinct seams, unless associated with an anhydrite layer, but are rather local horizontal concentrations of disseminated clay stringers. Therefore, computationally, seam properties can be ascribed to the concentration of clay. In the calculational model here, the clay seam shear response is specified by a coefficient of friction, μ=0.2. Of the thirteen clay seams labeled A through M, only the nine nearest the room labeled D through L are taken as active and included in the calculation.

The calculational model represents a slice through the center of the room length and consists of a space defined by the vertical symmetry plane through the middle of the room and by a vertical far-field boundary placed far into the salt. So the model is effectively a plane strain model – appropriate for comparison with measurements taken at room mid-length for the relatively long room. The upper and lower model extremes are defined as shown.

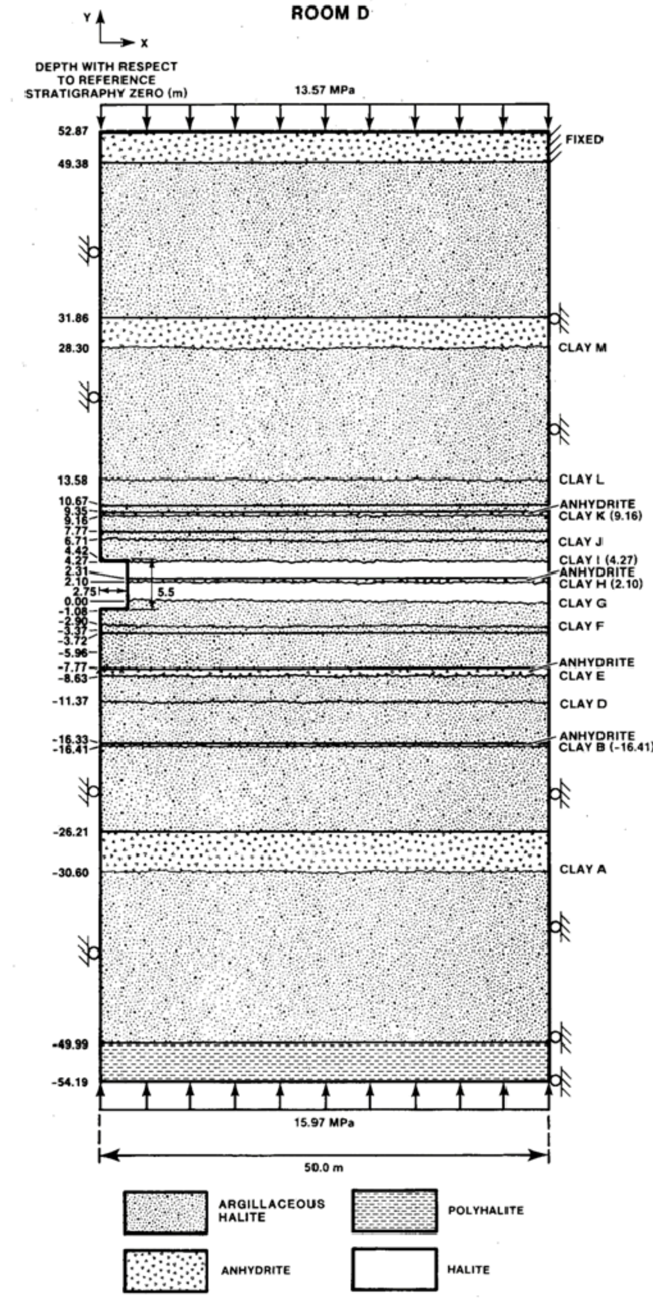

Fig. 6. Local stratigraphy around and model of Room D.

The boundaries, both vertical and horizontal, are sufficiently removed from the room that they cause an insignificant perturbation in stress or displacement at the room proper. Both of the vertical boundaries are constrained against horizontal (X-direction) movement, allowing only vertical displacements. The horizontal boundaries are traction boundaries. A uniform pressure of 13.57 MPa is applied at the upper horizontal boundary, accounting for the weight of the overburden. The thickness weighted average of the densities of the materials in the layers of the calculational model [15] yielded an average density in the model of 2300 kg/m^3. This density results in a uniform pressure of 15.97 MPa on the bottom horizontal boundary, and accounts for the presence of a room that is instantaneously mined. A lithostatic initial stress state that varies linearly with depth is assumed based on the average material density and a gravitational acceleration of 9.79 m/s^2. The room surfaces are traction-free and the upper right corner of the model is fixed against horizontal and vertical (X-Y) movement. Properties use for Clean and Argillaceous salt in the model are those shown in Table 1.

It should be noted that both this room and its heated counterpart, WIPP Room B, have been the subject of some recent attention from a benchmarking perspective, and the interested reader can find many more details regarding the rooms and some preliminary simulations in these references [21,22,23]. In addition, the US-German international benchmarking project briefly described in [19] was recently extended to allow the inclusion of these two rooms as additional benchmark exercises to be undertaken by the partners.

While this simulation generates many results of interest, only one component of room closure is presented here, for brevity. Figure 7 shows the computed vertical closure from the latest Sierra Mechanics calculations for Room D compared to measured vertical closure from the room. Vertical closure is the relative displacement of the roof to the floor at the room at the centerline of the room. Again, it can be seen that the computed results compare quite well with the measurements and demonstrates the applicability and validity of the modeling capability described here to repository-scale problems. The results shown here are consistent with the results of Munson and co-workers [5], which used earlier generations of the technology originally developed for WIPP. That technology has since been improved (with ~30 years of hardware and software improvements) and is embodied in the current state-of-the-art Sierra Mechanics computational capability.

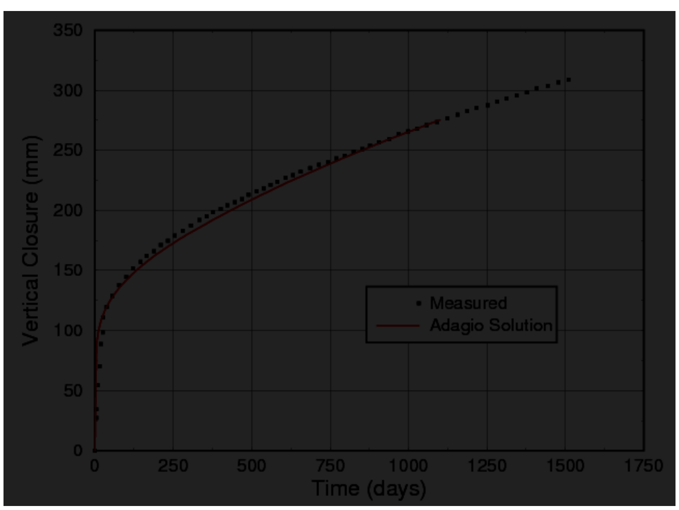

Fig. 7. WIPP Room D Model Vertical Closure Results vs. Measurements.

5. SUMMARY AND CONCLUSIONS

Because of relatively recent decisions by the current administration and its renewed assessment of the nuclear life-cycle, the various deep geologic disposal medium options are open for consideration once again. This paper has focused on addressing the favorable creep properties and behavior of geologic rock salt, from the computational modeling perspective, as it relates to its potential use as a medium for a deep geologic repository. The various components that make up a computational modeling capability to address the thermo-mechanical behavior of rock salt over a wide range of time and space have been presented. Several example salt calculations were also presented to demonstrate the applicability and validity of the modeling capability described to address repository-scale problems. These varied from simple problems designed to test elementary creep response behavior to the more complex that dealt with addressing specific aspects of repository room behavior. The evidence shown points to a mature computational capability that can generate results relevant to the design and assessment of a potential rock salt HLW repository. In fact the capability embodied within Sierra Mechanics has already been exercised and demonstrated, to a limited extent, via a scoping study of a generic HLW repository [24]. The computational capability described here can be used to help enable fuel cycle sustainability by appropriately vetting the use of geologic rock salt for use as a deep geologic disposal medium.

ACKNOWLEDGEMENTS

The author would like to acknowledge James Bean, John Holland, and Jonathan Rath for their many outstanding contributions to the calculational efforts summarized herein. The author is ultimately responsible for the contents of this paper; however, it would not have been possible without the professional dedicated contributions of these individuals. The author also acknowledges the USDOE NE/FCR&D Program for supporting this work. Sandia National Laboratories is a multi-program laboratory managed and operated by Sandia Corporation, a wholly owned subsidiary of Lockheed Martin Corporation, for the U.S. Department of Energy's National Nuclear Security Administration under contract DE-AC04-94AL85000.

REFERENCES

1. Nuclear Energy Institute (NEI). 2014. On-Site Storage of Nuclear Waste. http://www.nei.org/Knowledge-Center/Nuclear-Statistics/On-Site-Storage-of-Nuclear-Waste (last accessed on 2/17/2014).
2. National Research Council. 1957. Disposal of Radioactive Waste on Land. Committee on Waste Disposal; Division of Earth Sciences. National Academy of Sciences, Washington, D.C.

3. Blue Ribbon Commission on America's Nuclear Future (BRC). January 2012. Report to the Secretary of Energy. U.S. Department of Energy, Washington, D.C.

4. Waste Management Technology Department (WMTD). 1985. The Scientific Program at the Waste Isolation Pilot Plant, SAND85-1699, Sandia National Laboratories, Albuquerque, NM.

5. Munson, D. E. 1997. Constitutive Model of Creep in Rock Salt Applied to Underground Room Closure. *Int. J. Rock Mech. Min. Sci.* 34:2 233-247.

6. Munson, D.E. and P.R. Dawson. 1979. Constitutive Model for the Low Temperature Creep of Salt (With Application to WIPP). SAND79-1853, Sandia National Laboratories, Albuquerque, NM.

7. Munson, D.E. and P.R. Dawson. 1982. A Transient Creep Model for Salt during Stress Loading and Unloading, SAND82-0962, Sandia National Laboratories, Albuquerque, NM.

8. Munson, D.E. and P.R. Dawson. 1984. Salt Constitutive Modeling using Mechanism Maps, *1st International Conference on the Mechanical Behavior of Salt*, Trans Tech Publications, Clausthal, Germany.

9. Munson, D.E., A.F. Fossum, and P.E. Senseny. 1989. Advances in Resolution of Discrepancies between Predicted and Measured in Situ WIPP Room Closures, SAND88-2948, Sandia National Laboratories, Albuquerque, NM.

10. Munson, D.E. 1979. Preliminary Deformation-Mechanism Map for Salt (with Application to WIPP), SAND70-0079, Sandia National Laboratories, Albuquerque, NM.

11. Fossum, A.F., G.D. Callahan, L.L. Van Sambeek, and P.E. Senseny, 1988. How Should One-Dimensional Laboratory Equations be Cast in Three-Dimensional Form? *Key Questions in Rock Mechanics: Proceedings of the 29th U.S. Symposium on Rock Mechanics.* Brookfield, MA: McGraw-Hill.

12. Edwards, H.C. and J.R. Stewart. 2001. SIERRA: A Software Environment for Developing Complex Multi-Physics Applications. In *Proceedings of the First MIT Conference on Computational Fluid and Solid Mechanics*, ed. K.J. Bathe, 1147–1150. Amsterdam: Elsevier.

13. Biffle, J. H. 1993. JAC3D – A Three-Dimensional Finite Element Computer Program for the Nonlinear Quasistatic Response of Solids with the Conjugate Gradient Method, SAND87-1305, Sandia National Laboratories, Albuquerque, NM.

14. Stone, C. M. 1997. SANTOS – A Two-Dimensional Finite Element Program for the Quasistatic, Large Deformation, Inelastic Response of Solids, SAND90-0543, Sandia National Laboratories, Albuquerque, NM.

15. Krieg, R. D. 1984. Reference Stratigraphy and Rock Properties for the Waste Isolation Pilot Plant (WIPP) Project, SAND83-1908, Sandia National Laboratories, Albuquerque, NM.

16. Senseny, P. E. 1986. Triaxial Compression Creep Tests on Salt From the Waste Isolation Pilot Plant, SAND85-7261, Sandia National Laboratories, Albuquerque, NM.

17. Lowe, M.J.S. and N.C. Knowles. 1989. COSA II: Further benchmark exercises to compare geomechanical computer codes for salt. Final report No. EUR 12135 EN. ISBN 92-825-9943-4. Luxembourg: Office for Official Publications of the European Communities.

18. Argüello, J. G., J.F. Holland, and J.E. Bean. 2012. International Benchmark Calculations of Field Experiments at the Asse Salt Mine, SAND2012-8193, Sandia National Laboratories, Albuquerque, NM.

19. Hampel, A., J.G. Argüello, F.D. Hansen, R.M. Günther, K. Salzer, W. Minkley, K.-H. Lux, K. Herchen, U. Düsterloh, A. Pudewills, S. Yildirim, K. Staudtmeister, R. Rokahr, D. Zapf, A. Gährken, C. Missal, and J. Stahlmann. 2013. Bennchmark Calculations of the Thermo-Mechanical Behavior of Rock Salt – Results from a US-German Joint Project. In *Proceedings of the 47th US Rock Mechanics/ Geomechanics Symposium, San Francisco, June 23-26 2013,* ARMA 13-456. :ARMA.

20. Munson, D.E., R.L. Jones, D.L. Hoag, and J.R. Ball. 1988. Mining Development Test (Room D): In Situ Data Report (March 1984 – May 1988) Waste Isolation Pilot Plant (WIPP) Thermal/Structural Interactions Program, SAND88-1460. Sandia National Laboratories, Albuquerque, NM.

21. Argüello, J.G. and J.S. Rath. 2012. SIERRA Mechanics for Coupled Multi-Physics Modeling of Salt Repositories. In *Proceedings of the 7th Conference on the Mechanical Behavior of Salt, Paris, France, 16-19, April 2012*, eds. P. Bérest et al, 413-423. London: Taylor & Francis Group.

22. Rath, J.S. and J.G. Argüello. September 2012. Revisiting Historical Numerical Analyses of the Waste Isolation Pilot Plant (WIPP) Room B and D in-situ Experiments Regarding Thermal and Structural Response, SAND2012-7525, Sandia National Laboratories, Albuquerque, NM.

23. Argüello, J.G. and J.S. Rath. 2013. Revisiting the 1980's WIPP Room D and B In-Situ Experiments: Performing Thermo-Mechanical Simulations of Rock Salt Using a State-of-the-Art Code Suite. In *Proceedings of the 47th US Rock Mechanics/ Geomechanics Symposium, San Francisco, June 23-26 2013,* ARMA 13-370. :ARMA.

24. Stone, C.M., J.F. Holland, J.E. Bean, and J.G. Argüello. 2010. Coupled Thermal-Mechanical Analyses of a Generic Salt Repository for High-Level Waste. In *Proceedings of the 44th US Rock Mechanics Symposium, Salt Lake City, 27-30 June 2010*, ARMA 10-180. : ARMA.